Materials Today Physics 44 (2024) 101423

Contents lists available at ScienceDirect

Materials Today Physics

journal homepage: www.journals.elsevier.com/materials-today-physics

The relation between the atomic mass ratio and quartic anharmonicity in alkali metal hydrides

Minxuan Feng [a,1], Xiaoying Wang [a,1], Guimei Zhu [b,**], Cheng He [a], Jun Sun [a], Xiangdong Ding [a], Junichiro Shiomi [c], Yi Xia [d], Baowen Li [e], Zhibin Gao [a,*]

[a] State Key Laboratory for Mechanical Behavior of Materials, Xi'an Jiaotong University, Xi'an, 710049, China
[b] School of Microelectronics, Southern University of Science and Technology, Shenzhen, 518055, China
[c] Department of Mechanical Engineering, The University of Tokyo, Tokyo, 113-8656, Japan
[d] Department of Mechanical and Materials Engineering, Portland State University, Portland, OR, 97201, USA
[e] Department of Materials Science and Engineering, Department of Physics. Southern University of Science and Technology, Shenzhen, 518055, China

A B S T R A C T

Phonons play a crucial role in understanding various aspects of solid-state physics, including thermal expansion, phase transition, interfacial thermal resistance, and lattice thermal conductivity (κ_L). Usually, the three-phonon (3ph) scattering processes have been considered the dominant mechanism governing thermal transport in solids. However, recent studies have revealed that quartic anharmonicity can fill the gap between theoretical calculations based on 3ph interactions and experimental values in a range of materials, such as BAs, perovskite $CsPbBr_3$, and thermoelectric PbTe. Typically, the vibration frequency of phonons is proportional to the inverse square root of the atomic mass. Some semiconductors with heavy atoms have a big mass ratio which leads to a gap between acoustic and optical phonon modes. This phenomenon concurrently suppresses 3ph scattering. The influence of 4ph scattering on κ_L becomes more important. We investigate the relation between the atomic mass ratio and quartic anharmonicity using rocksalt alkali metal hydrides XH (X = Li, Na, K, Rb, Cs). Our finding reveals a positive correlation between the atomic mass ratio and quartic anharmonicity.

1. Introduction

The ability to understand and predict materials with either extremely high or extremely low thermal conductivity is of utmost importance in various fields, including thermoelectrics and thermal management. These materials play a critical role in applications such as heat dissipation, heat insulation, thermal regulation, and thermal cooling [1–4]. On one hand, materials with high thermal conductivity are desirable for enhancing heat dissipation in electronic devices. They enable efficient heat transfer and help prevent overheating, thereby improving the performance and reliability of electronic components [5–8]. On the other hand, materials with low thermal conductivity are widely used as thermal barrier coatings to provide insulation and reduce heat transfer [9–11]. They are also employed in thermoelectric devices, which convert waste heat into useable electrical energy [12–14].

The thermal properties of insulators and semiconductors are predominantly governed by phonons [6,15–18]. Most of the previous κ_L calculations considered only 3ph scattering because the results agree with experiments relatively well for many materials and calculations of four-phonon (4ph) even higher-order scatterings are computationally demanding. Nevertheless, the prediction of κ_L for BAs is more accurate after considering the 4ph calculations [7,19–21]. Meanwhile in some low κ_L materials such as cubic oxide and fluoride perovskites phonon transport properties are clearly influenced by the scattering of 4ph [22].

Higher-order phonon scattering has been extensively studied [23]. The pioneering work originally predicted the quantum mechanical four-phonon scattering rates and reduced thermal conductivity of diamond, silicon, and germanium [24]. By considering fourth-order anharmonicity, phonon-phonon scattering has been shown to bridge the gap between theory and experiment [25–28]. First-principles calculations of lattice dynamics consider only 3ph scattering for cubic BAs, which exhibits an ultrahigh κ_L of 2200 W m^{-1} K^{-1} at room temperature [7]. When adding 4ph scattering, its κ_L decreases to around 1400 W m^{-1} K^{-1} [29]. Later, experimental measurements on BAs [19–21] confirm the predictions [29]. Similarly, Θ-phase Tantalum Nitride (TaN) exhibits ultrahigh κ_L of 995 and 820 W m^{-1} K^{-1} at 300 K along the *a* and *c* axes, respectively. 4ph scattering is found to be significant and will suppress 40 % κ_L compared with only considering the 3ph scattering in the

* Corresponding author.
** Corresponding author.
E-mail addresses: zhugm@sustech.edu.cn (G. Zhu), zhibin.gao@xjtu.edu.cn (Z. Gao).
[1] These authors contributed equally to this work.

https://doi.org/10.1016/j.mtphys.2024.101423
Received 4 February 2024; Received in revised form 2 April 2024; Accepted 2 April 2024
Available online 15 April 2024

first-principle calculations [30].

In compounds like BAs and TaN, which contain heavy atoms (As and Ta, respectively), the heavier atoms result in lower phonon frequencies. This leads to a substantial gap between the optical and acoustic phonon branches [31]. Since each phonon scattering process must simultaneously satisfy energy and quasi-momentum conservation, a large acoustic-optical phonon gap will suppress AAO scatterings, where "A" stands for acoustic phonons and "O" means optical phonons [32–34]. Therefore, a large A-O gap commonly inhibits 3ph scatterings [29]. When 3ph scattering is suppressed, 4ph scattering becomes relatively more prominent in the total phonon scattering processes. Consequently, a natural question arises: does the increased atomic mass ratio in compounds correlate with a higher significance of quartic anharmonicity? The pioneering work studied the 4ph and normal scattering combined with the mass ratio in 2D hexagonal structures (graphene, BN, AlN, and GaN) which are all high thermal conductivity materials. Our work focuses on low thermal conductivity materials with different mass ratios. Besides, our work not only considers the four-phonon scattering but also evaluates the phonon renormalization as a function of the temperature [35].

We investigate the relationship between the atomic mass ratio and quartic anharmonicity, by using a series of rocksalt alkali metal hydrides XH (X = Li, Na, K, Rb, Cs) compounds. The atomic mass of hydrogen is unity, and the mass ratio can be gradually increased by replacing the metal X atom. All the binary compounds XH have isotropic cubic structures with $Fm\bar{3}m$ (space group no. 225), which are commonly used for hydrogen storage [36–40] and superconducting [41].

2. Computational methods

We utilized *ab initio* density functional theory as implemented in VASP combined with projector-augmented wave (PAW) pseudopotentials [42] and the Perdew-Burke-Ernzerhof (PBE) functionals [43]. A cutoff energy of 650 eV and convergence thresholds of 10^{-4} eV/Å for Hellmann-Feynman forces in each atom and 10^{-8} eV for total energy were used. A 4 × 4 × 4 supercell and a 11 × 11 × 11 Monkhorst-Pack *k*-grids were used to generate second-order interatomic force constants (IFCs) by the finite-displacement technique. Subsequently, we ran 2000-step *ab initio* molecular dynamics (AIMD) at 300 K with 2 ps step size and selected 30 random and incoherent configurations. Then we used compressive sensing lattice dynamics (CSLD) [44,45] to obtain third- and fourth-order IFCs. Combining all IFCs together [46], we can calculate the thermal transport properties of XH.

Using a Taylor expansion with respect to displacement from the equilibrium position at zero temperature, the interatomic potential can be expressed

$$U = U_0 + \sum_{N=2}\frac{1}{N!}\sum_{\boldsymbol{m}_1\alpha_1,\ldots,\boldsymbol{m}_N\alpha_N}\sum_{\mu_1,\ldots,\mu_N}\boldsymbol{\Phi}^{\mu_1,\ldots,\mu_N}_{\boldsymbol{m}_1\alpha_1,\ldots,\boldsymbol{m}_N\alpha_N} \times u^{\boldsymbol{m}_1\alpha_1}_{\mu_1}\ldots u^{\boldsymbol{m}_N\alpha_N}_{\mu_N}, \tag{1}$$

where μ_i, $\boldsymbol{m}_i$, and α_i are *xyz* components, translation vector in the primitive cell, and atomic index in the $\boldsymbol{m}_i$ unit cell, respectively. $\boldsymbol{u}^{\mu}_{\boldsymbol{m}\alpha}$ stands for the displacement of atom α along μ direction in the unit cell $\boldsymbol{m}$. The IFCs are defined as,

$$\boldsymbol{\Phi}^{\mu_1,\ldots,\mu_N}_{\boldsymbol{m}_1\alpha_1,\ldots,\boldsymbol{m}_N\alpha_N} = \frac{\partial^N V}{\partial u^{\mu_1}_{\boldsymbol{m}_1\alpha_1}\ldots\partial u^{\mu_N}_{\boldsymbol{m}_N\alpha_N}}, \tag{2}$$

in which $N = 2$ is the harmonic and $N \geq 3$ is called anharmonic lattice model. The 4ph scatterings must involve truncation order $N_{\max} = 4$, while 3ph only needs $N_{\max} = 3$. The lattice thermal conductivity κ_L can be obtained by the linearized Boltzmann transport equation (BTE) [11],

$$\kappa_L^{\alpha\beta} = \frac{1}{8\pi^3}\int_{BZ}\sum_{p} C_V(p\boldsymbol{q})v^{\alpha}_{p\boldsymbol{q}}F^{\beta}_{p\boldsymbol{q}}d^3\boldsymbol{q}, \tag{3}$$

where $C_V(p\boldsymbol{q})$, $v^{\alpha}_{p\boldsymbol{q}}$ and $F^{\beta}_{p\boldsymbol{q}}$ are isobaric heat capacity, group velocity and phonon mean free path, respectively. p and $\boldsymbol{q}$ are phonon branch index and wave vector.

$$F^{\beta}_{p\boldsymbol{q}} = \tau_{p\boldsymbol{q}}(v^{\beta}_{p\boldsymbol{q}} + \Delta^{\beta}_{p\boldsymbol{q}}), \tag{4}$$

in which $\tau_{p\boldsymbol{q}}$ is the phonon relaxation time and $\Delta^{\beta}_{p\boldsymbol{q}}$ depicts the quantity away from the relaxation time approximation (RTA). The converged result of $F^{\beta}_{p\boldsymbol{q}}$ can be obtained by the calculation of BTE iteratively [46]. Furthermore, the total scattering rates of phonons are the summation of several scattering mechanisms, such as three-phonon, four-phonon, phonon-isotope, and electron-phonon scattering. $\frac{1}{\tau_{p\boldsymbol{q}}} = \frac{1}{\tau^{3ph}_{p\boldsymbol{q}}} + \frac{1}{\tau^{4ph}_{p\boldsymbol{q}}} + \frac{1}{\tau^{ph-iso}_{p\boldsymbol{q}}} + \frac{1}{\tau^{el-ph}_{p\boldsymbol{q}}}$. Here, we consider intrinsic 3ph and 4ph scatterings.

The effect of fourth-order anharmonicity mainly divides into two parts. One is the adding term of 4ph scattering $1/\tau^{4ph}_{p\boldsymbol{q}}$ that will increase $1/\tau_{p\boldsymbol{q}}$ and decrease κ_L. The other one is the change of the phonon spectrum [47,48], which will modify the phonon group velocity $v^{\alpha}_{p\boldsymbol{q}}$ and phonon lifetime $\tau_{p\boldsymbol{q}}$ accordingly.

To include the temperature-dependent phonon frequency shift, we use the self-consistent phonon theory (SCPH) [45,49], which can take quartic anharmonicity into consideration. The phonon frequency shift can be expressed as [50],

$$\Omega^2_{\lambda} = \omega^2_{\lambda} + 2\Omega_{\lambda}\sum_{\lambda_1} I_{\lambda\lambda_1}, \tag{5}$$

where λ and ω_{λ} are the phonon modes and phonon frequency by the harmonic approximation. Ω_{λ} is the temperature-dependent phonon frequency which is renormalized from quartic anharmonicity and temperature. The $I_{\lambda\lambda_1}$ is [50],

$$I_{\lambda\lambda_1} = \frac{\hbar}{8N_0}\frac{V^{(4)}(\lambda,-\lambda,\lambda_1,-\lambda_1)}{\Omega_{\lambda}\Omega_{\lambda_1}}[1 + 2n_{\lambda}(\Omega_{\lambda_1})], \tag{6}$$

Parameter $V^{(4)}(\lambda, -\lambda, \lambda_1, -\lambda_1)$ is the reciprocal representation of the fourth-order IFCs. The n_{λ} is phonon population which satisfies Bose-Einstein distribution as a function of the temperature.

The paper is organized as follows: in section I, we present the temperature-dependent κ_L. In section II, we illustrate the phonon dispersion and the shift of the frequency gap between the optical and acoustic phonon branches. In section III, we reveal the relation between the atomic mass ratio and quartic anharmonicity. In section IV, we investigate the physical mechanism of quartic anharmonicity as a function of the atomic mass ratio.

3. Thermal conductivity vs temperature

The quartic anharmonicity accounts for both four-phonon scattering rates and phonon frequency shifts. Our entire calculation framework is grounded in the self-consistent phonon (SCPH) theory, which represents an alternative approach for incorporating strong anharmonic effects beyond perturbation theory. SCPH method comprehensively considers the quantum effects of phonons, a concept that has been extensively discussed in pioneering works [44,45,48,52]. For a polar solid, the atomic forces can be divided into two additive contributions: analytic and non-analytic. The analytic term accounts for all the forces under the restricted periodic boundary conditions under which the averaged electric field is assumed to be zero. The non-analytic contribution accounts for the additional forces owing to a nonzero-averaged electric field. We consider the LO-TO splitting for polar XH compounds in our whole calculations [53].

In previous work, theoretical data of LiH are 23.0 W m^{-1} K^{-1} [54]

and 18.3 W m^{-1} K^{-1} [48], very close to our computational result of 19.7 W m^{-1} K^{-1} for LiH. The experimental κ_L of LiH are 12.47 W m^{-1} K^{-1} [54] and 14.7 W m^{-1} K^{-1} [48] at 300 K. The error between experimental data and calculations is probably from the impure and polycrystalline samples.

In Fig. 1(a)-(d), we discover that κ_L of approximation model considering 3ph (red dotted lines) always exceed the model considering 3ph and 4ph (red lines), attributed to the additional 4ph scattering which enhances the phonon scattering rates and scattering phase space.

In Fig. 1(a)–(d), the SCPH+3ph (blue dotted lines) are always above HA+3ph (the red dotted lines). And in Fig. 1(e), the SCPH+3ph (blue dotted lines) are below HA+3ph (the red dotted lines). The thermal conductivity of CsH reduces after considering the SCPH method which is different from the other four XH materials in Fig. 1 (e). The reason is the acoustic branch of CsH tends to soften with increasing temperatures shown in Fig. 2. The thermal conductivity is mainly contributed by the acoustic branch as shown in Fig. 5 (b). The softened acoustic branch of CsH leads to group velocity decreases shown in Supplemental Material Fig. S2 which reduces the thermal conductivity. We will discuss the difference of phonon spectrum in detail in Section II. Three conclusions for various XH materials are summarized as follows:

(1) For a given temperature, κ_L is decreased with the mass of the heavier atom increasing in various materials; (2) For the same material, κ_L is decreased when the temperature is increased due to the enhanced phonon-phonon scatterings; (3) $\Delta\kappa = \kappa_{3ph}^{SCPH} - \kappa_{3,4ph}^{SCPH}$ increases as the temperature is increased for all XH materials.

For the same materials, 4ph becomes dominant due to the enhanced phonon-phonon scatterings at elevated temperatures. It is essential to note that the rates of 3ph scattering are proportional to the temperature T, while those of 4ph scattering are roughly proportional to T^2 [29,55]. Due to this quadratic dependence, the 4ph scattering rates increase at a faster rate with increasing temperature compared to the 3ph scattering rates. Consequently, at higher temperatures, the contribution of 4ph processes becomes more significant.

4. The phonon dispersion and the frequency shift

To investigate the physical correlation between the larger atomic mass ratio and quartic anharmonicity, we show phonon dispersions of XH compounds considering quartic anharmonicity in Fig. 2(a)–(e), which reveals the phonon frequency shifts by renormalized phonons [50]. In LiH, whole phonon frequencies are stiffening with the temperature increasing no matter what they are acoustic phonons or optical phonons. A similar trends are observed in other XH materials except for CsH.

Remarkably, optical branches of CsH tend to harden, while acoustic branches become soft with increasing temperatures, as presented in Fig. 2(e). To explore the physical mechanism of the acoustic branches and optical branches having opposite temperature dependence, we introduce the 4ph interaction matrix elements $I_{\lambda\lambda_1}$ as shown in Eq. (5) and Eq. (6). $I_{\lambda\lambda_1}$ is mainly negative for the TA mode in CsH as shown in Fig. 3(a). In contrast, it is found that the $I_{\lambda\lambda_1}$ of LO mode is mainly positive. Because the $I_{\lambda\lambda_1}$ can be negative or positive, the temperature-dependent phonon frequency Ω_λ can be increase or decrease which leads to the different variations of phonon spectrum in CsH [48,50]. The reason behind this unique behavior may be attributed to a kind of low-temperature strong phonon anharmonic effect of cesium compounds that were also presented in cesium chloride (CsCl) [56–58].

Fig. 2(f) illustrates the changes in $\Delta\omega/\omega_A$, where $\Delta\omega = \omega_O - \omega_A$ represents the frequency gap between the lowest optical phonon branch and the highest acoustic phonon branch. Both the 3ph and 4ph scatterings must satisfy energy and quasi-momentum conservation simultaneously. If the $\Delta\omega$ value is large enough, the sum of two acoustic phonons frequencies is unable to reach that of one optical phonon (for an AAO phonon scattering process). Consequently, leading the

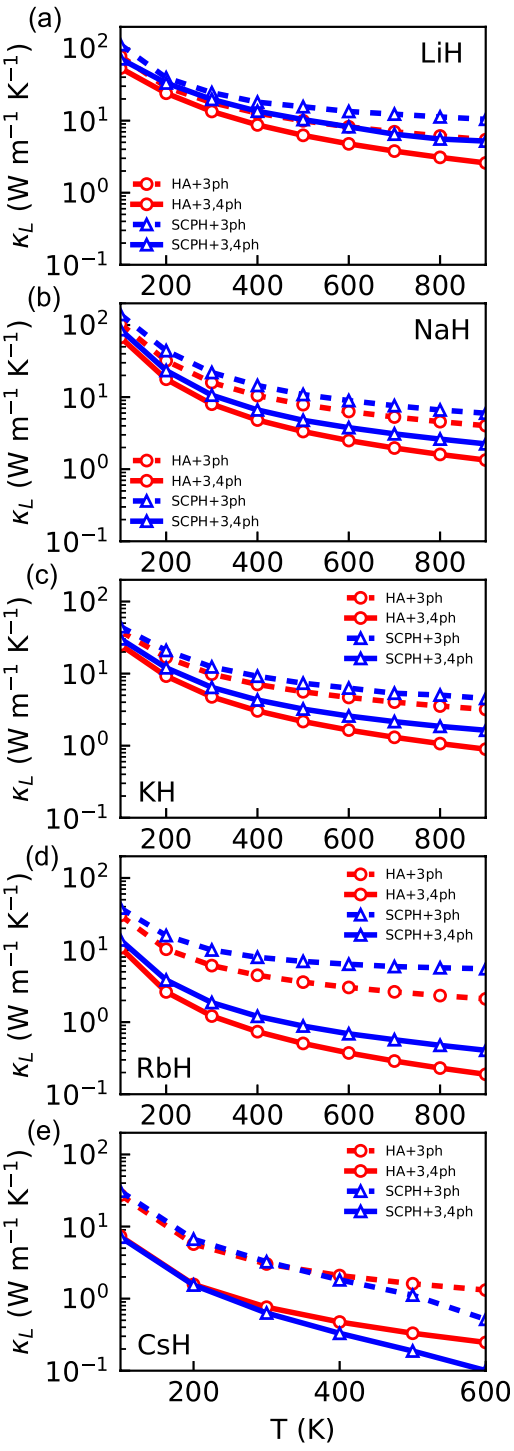

Fig. 1. κ_L for XH materials by considering the LO-TO splitting. (a) LiH, (b) NaH, (c) KH, (d) RbH, and (e) CsH. The dotted red lines represent κ_L only considering the harmonic approximation and three-phonon scattering (HA+3ph). The red lines show κ_L including three-phonon and four-phonon scatterings (HA+3,4ph). Blue dotted lines stand for κ_L having self-consistent phonon approximation which includes anharmonic renormalization due to quartic anharmonicity, in conjunction with three-phonon scattering (SCPH+3ph). Blue lines denote that one with both 3ph and 4ph scattering (SCPH+3ph+4ph). (For interpretation of the references to color in this figure legend, the reader is referred to the Web version of this article.)

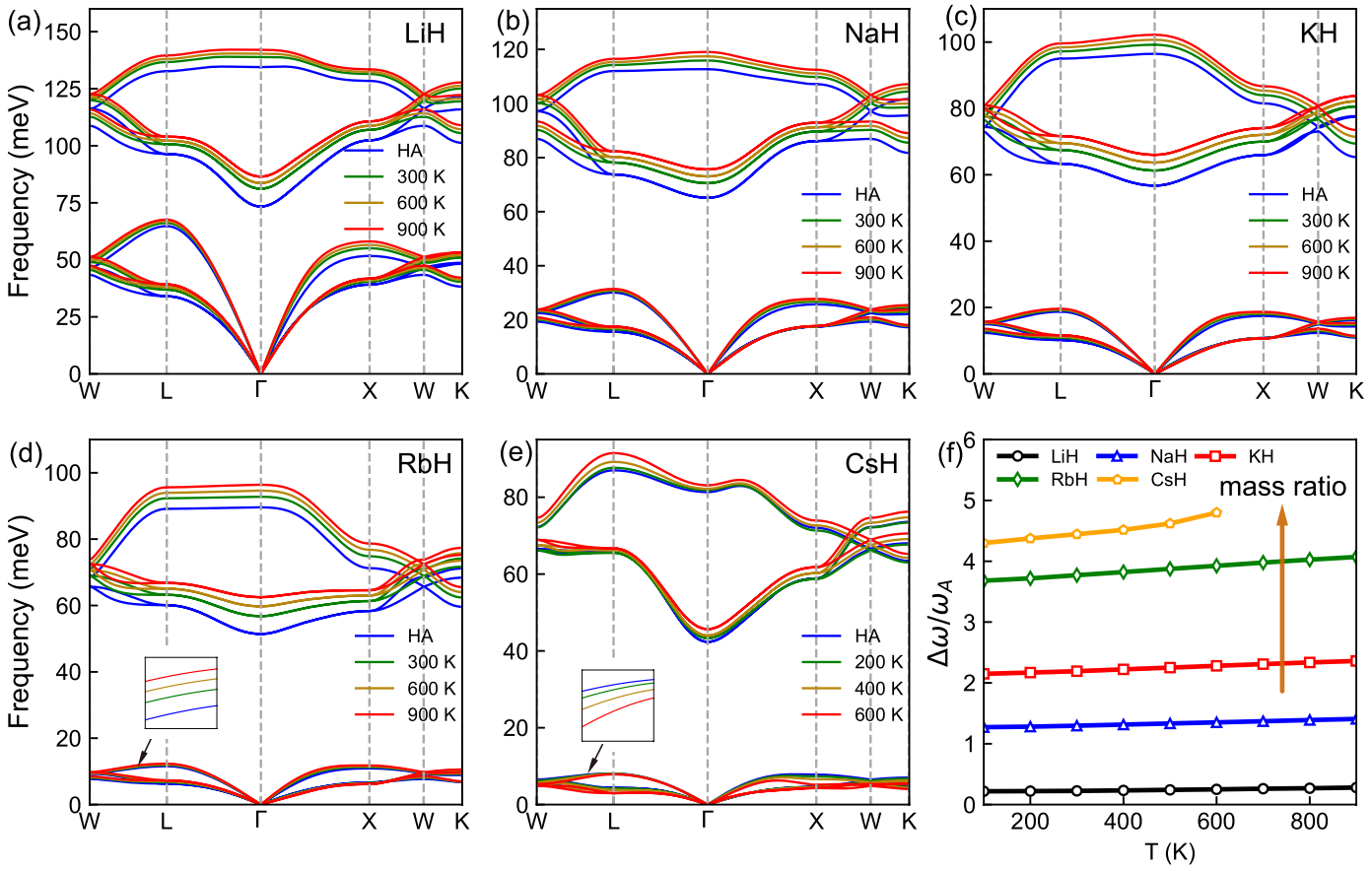

Fig. 2. The phonon dispersions of XH materials after considering the LO-TO splitting, (a) LiH, (b) NaH, (c) KH, (d) RbH, (e) CsH, respectively. The blue lines represent the phonon dispersions only considering the harmonic approximation. The green, yellow, and red lines reflect anharmonic renormalization at 300 K, 600 K, and 900 K, respectively, except for CsH where the colors represent 200 K, 400 K, and 600 K. Since the melting point of CsH is around 795.15 K [51], we choose low temperatures for the CsH material. The phonon dispersion of CsH at 700 K has imaginary frequencies. (f) The relative frequency change, $\Delta\omega = \omega_O - \omega_A$, $\Delta\omega/\omega_A$ in XH materials as a function of temperature. Here, ω_O and ω_A correspond to the lowest frequency of the optical branch and the highest frequency of the acoustic branch, respectively. (For interpretation of the references to color in this figure legend, the reader is referred to the Web version of this article.)

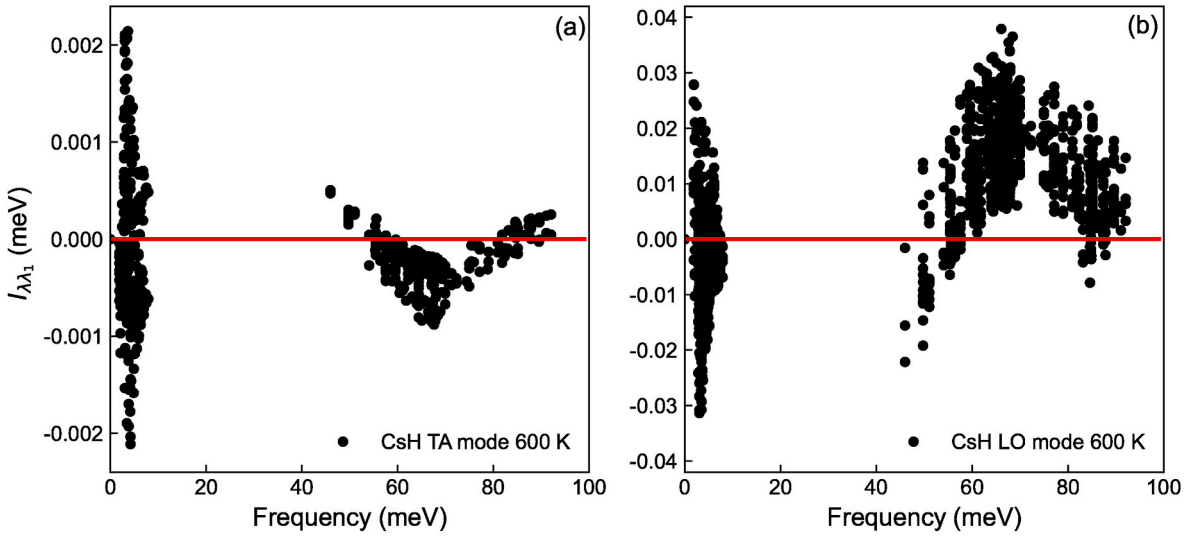

Fig. 3. Scattering strength of $I_{\lambda\lambda_1}$ 4ph interaction matrix elements between TA (LO) and all other phonons in CsH at 600 K around L high-symmetry points.

likelihood of the AAO scattering channel will be restricted [11,32]. The $\Delta\omega/\omega_A$ value tends to increase as the atomic mass becomes larger for different materials. Moreover, the largest optical phonon frequency typically decreases as the atomic mass of X atom increases, according to $1/\sqrt{m}$. Thus, regulating the $\Delta\omega/\omega_A$ value in binary XH compounds can be achieved by adjusting the atomic mass accordingly.

For the same material, the value of $\Delta\omega/\omega_A$ tends to increase with higher temperatures, as demonstrated in Fig. 2(f). As temperature

increases, the frequency of the optical branch notably increases, while the variation of the acoustic branch can be neglected. This indicates that the optical phonons in XH compounds are more sensitive to the change of temperature than the acoustic phonons. The rise in $\Delta\omega/\omega_A$ can be interpreted as the phonon frequency shift resulting from quartic phonon anharmonicity. Consequently, the impact of the quartic phonon anharmonicity becomes more prominent with increasing temperatures for the same material of the XH system indicated by $\Delta\omega/\omega_A$ values.

5. The atomic mass ratio and quartic anharmonicity

In Fig. 1, we have shown the variation of κ_L with temperature which consider 4ph scattering and renormalized phonon frequency shift. But it does not directly answer the question we posed. Next, we use $\kappa^{HA}_{3,4ph}/\kappa^{HA}_{3ph}$ and $\kappa^{SCPH}_{3,4ph}/\kappa^{HA}_{3ph}$ to discuss the influence of quartic anharmonicity.

In Fig. 4(a), the ratio of $\kappa^{HA}_{3,4ph}/\kappa^{HA}_{3ph}$ is presented, which provides insight into the impact of 4ph scattering. Compared to the result obtained from 3ph scattering, considering 4ph scattering can increase the phonon-phonon scattering and enhance the scattering phase space, leading to a decrease of κ_L. As a result, the ratio of $\kappa^{HA}_{3,4ph}/\kappa^{HA}_{3ph}$ shown in Fig. 4(a) is less than one. For instance, κ_L of RbH at 900 K, red bar in Fig. 4(a), decreases to 8.98 % after considering the 4ph scattering. It is obvious that $\kappa^{HA}_{3,4ph}/\kappa^{HA}_{3ph}$ decreases as the atomic mass of the X atom increases in XH binary compounds. This means that 4ph scattering becomes more and more important with the increased atomic mass ratio. Interestingly, CsH is an anomalous material that appears to be contrary to the other XH systems when considering $\kappa^{HA}_{3,4ph}/\kappa^{HA}_{3ph}$.

In Fig. 4(b), we discuss the consequence of quartic anharmonicity, which includes both 4ph scattering and phonon frequency shift. Here, $\kappa^{SCPH}_{3,4ph}$ refers to 3ph, 4ph and self-consistent phonon scatterings. The effect of 4ph scattering decreases κ_L, whereas phonon frequency shift increases the second-order phonon frequencies and finally enhances κ_L. The combination of these two effects on κ_L makes the variation of $\kappa^{SCPH}_{3,4ph}/\kappa^{HA}_{3ph}$ complicated. Therefore, in Fig. 4(b), some materials of $\kappa^{SCPH}_{3,4ph}/\kappa^{HA}_{3ph}$ are greater than one, and some materials of $\kappa^{SCPH}_{3,4ph}/\kappa^{HA}_{3ph}$ are less than one.

The quartic anharmonicity includes 4ph scattering and phonon frequency shift which affects the phonon lifetime and group velocities [48]. As a consequence, the influence of both factors on κ_L is not a simple summation but a complex coupling. For the different XH materials, the effect of quartic anharmonicity becomes more dominant as the atomic mass ratio increases.

6. The physical mechanism

To analyze the intrinsic mechanism of the atomic mass ratio and quartic anharmonicity, we investigate the scattering phase space and the scattering rates which both are shown in the Supplemental Material. The phase space of renormalized 4ph increases as the atomic mass ratio increases shown in Fig. 5(a). This indicates that the available scattering channels of 4ph increase when the atomic mass ratio increases in XH compounds. To further understand the influence of quartic anharmonicity, we show the scattering rates for XH materials in Supplemental Material Fig. S3. We find the magnitude of 4ph scattering rates are close to the 3ph in the same XH material. Since it is difficult to compare the importance of 4ph as illustrated in Fig. S3 directly, we use the ratio of scattering rates (α_4/α_3) to illustrate the importance of quartic anharmonicity in different XH materials.

The phonon spectrum, especially for the optical branch of XH materials, changes significantly as the atomic mass ratio increases. Thus we investigate the cumulative κ_L as a function of phonon frequency. As shown in Fig. 5(b), κ_L is mainly contributed by acoustic phonons for all XH materials. For LiH, NaH, KH, RbH, and CsH, the largest phonon frequencies that contribute the most to κ_L are 25.9 meV, 16.3 meV, 9.9 meV, 7.1 meV, and 2.9 meV, respectively. Therefore, we focus on the scattering rates of the corresponding phonon frequency range.

As the mass ratio of XH materials increases, the ratio of scattering rates α_4/α_3 tends to increase as displayed in Fig. 5(c). The contribution of 4ph scattering rates becomes more and more important in κ_L with larger atomic mass ratio at the corresponding frequency range. These evidence suggests that larger atomic mass ratios enhance the 4ph scattering rates and temperature-dependent renormalized phonon effects. Therefore, the phonon-phonon scattering rates and phonon phase space of the fourth-order phonon interactions become more important as the mass ratio increases in XH materials, leading to a dominated quartic anharmonicity.

7. Summary and discussion

In response to our initial question, we have summarized that $\kappa^{SCPH}_{3,4ph}/\kappa^{HA}_{3ph}$ decrease as the atomic mass ratio increases. The effect of quartic anharmonicity which includes 4ph scattering rates and the temperature-induced phonon frequency shift [48] becomes more important as the atomic mass ratio increases. It has certificated that the larger atomic mass ratio, the more crucial role of quartic anharmonicity in XH compounds. These results offer insights into the regularity of quartic anharmonicity affecting κ_L and shed light on the underlying

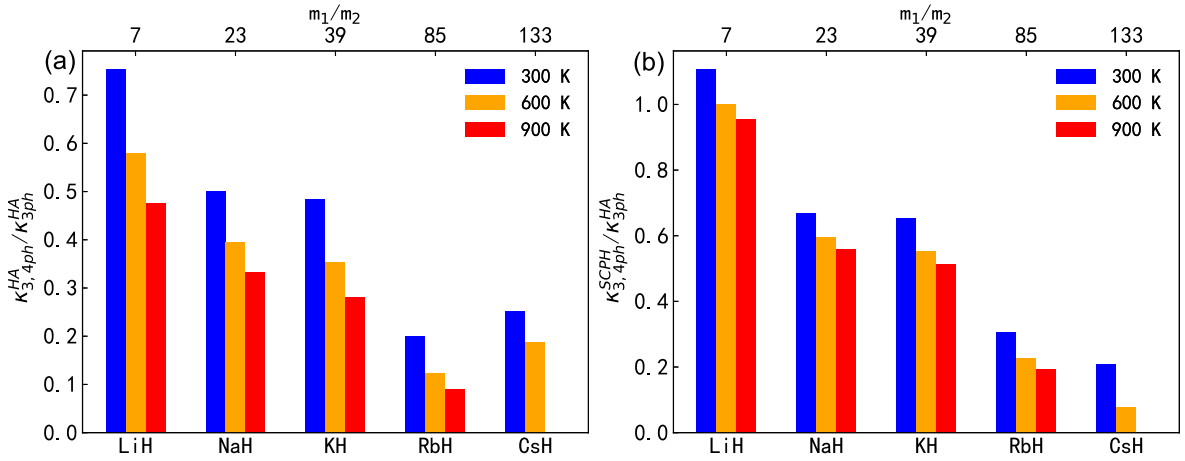

Fig. 4. κ_L of XH materials is presented using different theories after considering the LO-TO splitting. Specifically, κ^{HA}_{3ph} refers to the harmonic approximation without phonon renormalization. $\kappa^{HA}_{3,4ph}$ refers to the calculations considering both 3ph and 4ph scatterings. $\kappa^{SCPH}_{3,4ph}$ represents the calculations accounting for 3ph, 4ph scattering, and self-consistent phonon methods. The figure presents the ratios of (a) $\kappa^{HA}_{3,4ph}/\kappa^{HA}_{3ph}$ and (b) $\kappa^{SCPH}_{3,4ph}/\kappa^{HA}_{3ph}$ at different temperatures.

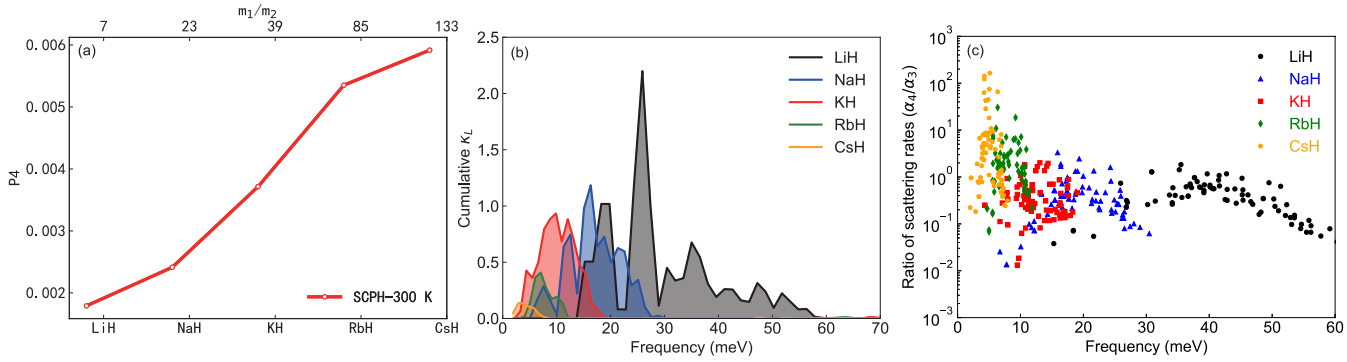

Fig. 5. (a) The total volume in phase space available for the four-phonon scattering processes (P4) which consider the self-consistent phonon at 300 K. (b) Cumulative κ_L of XH materials. (c) Ratio of scattering rates (α_4/α_3) for XH materials where $\alpha_4 = 1/\tau_4$ and $\alpha_3 = 1/\tau_3$. The ratio of α_4/α_3 are calculated for each phonon wave vectors and phonon branches.

physical mechanisms of 3ph, 4ph, and anharmonic phonon renormalization. Overall, our work provides a theoretical support for the rapid determination of the significance of quartic anharmonicity.

In general, the frequency shift can be caused by both 3ph scattering, 4ph scattering and thermal expansion. The effect of the 4ph frequency shift has been described in detail in Section II. Here, We give some discussion about the 3ph scattering and thermal expansion (see Fig. 6).

In the phonon frequency shift, the three-phonon scattering contributes to the second-order bubble diagram, while the four-phonon scattering contributes to the first-order loop diagram [47,59]. Usually, the frequency shift from the three-phonon scattering is negligible. Besides, our XH system satisfies the lattice translational invariance, which would lead to the zero frequency shift from the three-phonon scattering [60]. We also quantitatively calculate the frequency shift of 3ph in LiH at 300 K as shown in Fig. 6(a), which further proves the effect of 3ph on frequency shift can be negligible.

On the other hand, we calculate the phonon frequency shift by the thermal expansion. First, we check the thermal expansion coefficients of LiH (4.2×10^{-5} K^{-1} [61]) measured by the experiment. Then, we can obtain the accurate lattice constant for a given temperature. The initial lattice constant of LiH is 3.997 Å (structure optimization using PBE) at 0 K. Therefore, the lattice constants of LiH at 300 K and 600 K are 4.047 Å and 4.098 Å, respectively.

Next, we use these two different lattice constants of LiH to compute the phonon dispersions and quartic phonon renormalization, as shown in Fig. 6(b). Thermal expansion does have some effect on phonon frequency shift, and the higher the temperature, the greater the effect. Since LiH has a positive thermal expansion coefficient, the lattice constant at high temperatures will decrease. Consequently, the thermal expansion softens the phonon modes. The red and blue lines are lower than the black line around Γ point. However, after considering both thermal expansion and four-phonon renormalization, the phonon frequency becomes harder. The green and orange lines are higher than the black line. As a result, the four-phonon anharmonicity is more important than the thermal expansion effect on the phonon frequency shift.

The total calculation of three-phonon scattering, four-phonon scattering, and anharmonic phonon renormalization including the thermal expansion effect for all five XH materials (X = Li, Na, K, Rb, and Cs) is computationally prohibitive. Our present work focuses on the mass ratio and quartic anharmonicity. We believe thermal expansion, to a certain extent, will change the phonon frequency quantitatively. However, it does not change the direct proportional relationship between quartic anharmonicity and the atomic mass ratio.

CRediT authorship contribution statement

Minxuan Feng: Writing – original draft, Visualization. **Xiaoying Wang:** Writing – original draft, Visualization. **Guimei Zhu:** Writing –

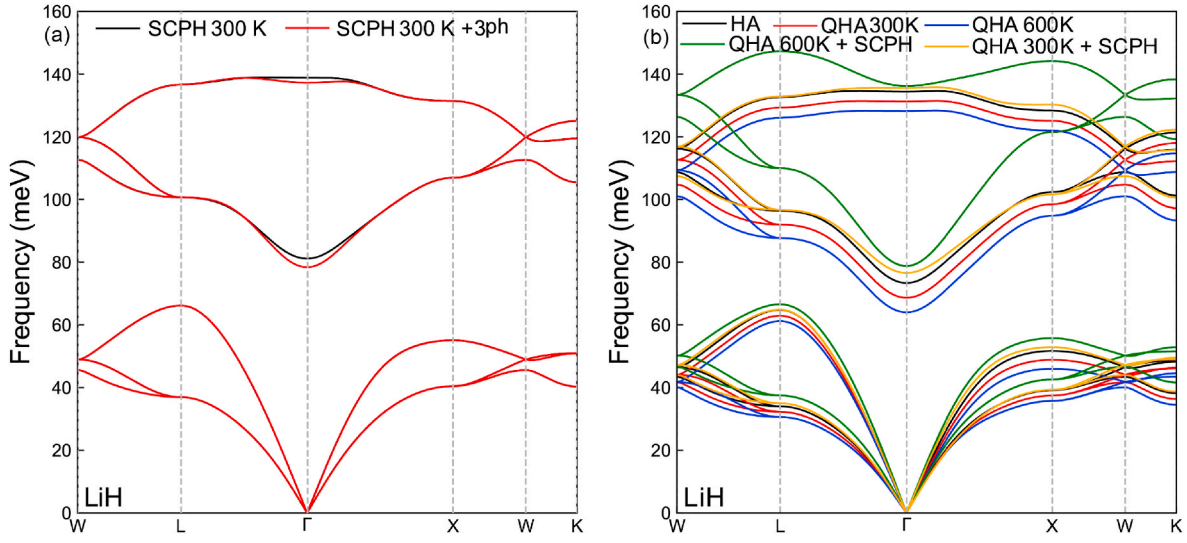

Fig. 6. The phonon dispersions for LiH. (a) The black lines represent the frequency shift from 4ph. The red lines represent the frequency shift from 3ph to 4ph. (b) The red lines and the blue lines show the frequency shift from thermal expansion at 300 K and 600 K of LiH. The orange lines and green lines represent the frequency shift from thermal expansion and 4ph.

review & editing. **Cheng He:** Writing – review & editing. **Jun Sun:** Writing – review & editing. **Xiangdong Ding:** Writing – review & editing. **Junichiro Shiomi:** Writing – review & editing. **Yi Xia:** Writing – review & editing. **Baowen Li:** Writing – review & editing. **Zhibin Gao:** Writing – review & editing, Writing – original draft, Validation, Supervision, Formal analysis, Data curation, Conceptualization.

Declaration of competing interest

The authors declare that they have no known competing financial interests or personal relationships that could have appeared to influence the work reported in this paper.

Data availability

Data will be made available on request.

Acknowledgements

The authors gratefully acknowledge discussions with Xiaolong Yang, Tianli Feng, Zhen Tong, and Liangfeng Huang.

We acknowledge the support of the National Natural Science Foundation of China (No. 12104356, No. 52250191, No. 52271113), China Postdoctoral Science Foundation (No. 2022M712552), the Opening Project of Shanghai Key Laboratory of Special Artificial Microstructure Materials and Technology (Ammt2022B-1), and the Fundamental Research Funds for the Central Universities. The work is supported by the Key Research and Development Program of the Ministry of Science and Technology under Grant No. 2023YFB4604100. Y.X. acknowledges Portland State University Lab Setup Fund. We also acknowledge the support by HPC Platform, Xi'an Jiaotong University.

Appendix A. Supplementary data

Supplementary data to this article can be found online at https://doi.org/10.1016/j.mtphys.2024.101423.

References

[1] Giulio Casati, Joseph Ford, Franco Vivaldi, William M. Visscher, One-dimensional classical many-body system having a normal thermal conductivity, Phys. Rev. Lett. 52 (1984) 1861–1864.
[2] Hongyi Ouyang, Yuanqing Gu, Zhibin Gao, Lei Hu, Zhen Zhang, Jie Ren, Baowen Li, Jun Sun, Yan Chen, Xiangdong Ding, Kirigami-inspired thermal regulator, Phys. Rev. Appl. 19 (2023): L011001.
[3] Eric S. Toberer, Lauryn L. Baranowski, Chris Dames, Advances in thermal conductivity, Annu. Rev. Mater. Res. 42 (2012) 179–209.
[4] Xin Qian, Jiawei Zhou, Gang Chen, Phonon-engineered extreme thermal conductivity materials, Nat. Mater. 20 (2021) 1188–1202.
[5] Lon E. Bell, Cooling, heating, generating power, and recovering waste heat with thermoelectric systems, Science 321 (2008) 1457–1461.
[6] Nianbei Li, Jie Ren, Lei Wang, Gang Zhang, Peter Hänggi, Baowen Li, Colloquium: phononics: Manipulating heat flow with electronic analogs and beyond, Rev. Mod. Phys. 84 (2012) 1045–1066.
[7] L. Lindsay, D.A. Broido, T.L. Reinecke, First-principles determination of ultrahigh thermal conductivity of boron arsenide: a competitor for diamond? Phys. Rev. Lett. 111 (2013): 025901.
[8] Savas Berber, Young-Kyun Kwon, David Tománek, Unusually high thermal conductivity of carbon nanotubes, Phys. Rev. Lett. 84 (2000) 4613–4616.
[9] Robert Vaßen, Maria Ophelia Jarligo, Tanja Steinke, Daniel Emil Mack, Detlev Stöver, Overview on advanced thermal barrier coatings, Surf. Coating. Technol. 205 (2010) 938–942.
[10] Bin Liu, Yuchen Liu, Changhua Zhu, Huimin Xiang, Hongfei Chen, Luchao Sun, Yanfeng Gao, Yanchun Zhou, Advances on strategies for searching for next generation thermal barrier coating materials, J. Mater. Sci. Technol. 35 (2019) 833–851.
[11] Zhibin Gao, Tao Fang, Jie Ren, Unusually low thermal conductivity of atomically thin 2D tellurium, Nanoscale 10 (2018) 12997–13003.
[12] Li-Dong Zhao, Shih-Han Lo, Yongsheng Zhang, Hui Sun, Gangjian Tan, Ctirad Uher, Christopher Wolverton, Vinayak P. Dravid, Mercouri G. Kanatzidis, Ultralow thermal conductivity and high thermoelectric figure of merit in SnSe crystals, Nature 508 (2014) 373–377.
[13] Gangjian Tan, Li-Dong Zhao, Mercouri G. Kanatzidis, Rationally designing high-performance bulk thermoelectric materials, Chem. Rev. 116 (2016) 12123–12149.
[14] Zhibin Gao, Gang Liu, Jie Ren, High thermoelectric performance in two-dimensional tellurium: an *ab initio* study, ACS Appl. Mater. Interfaces 10 (2018) 40702–40709.
[15] M.G. Holland, Phonon scattering in semiconductors from thermal conductivity studies, Phys. Rev. 134 (1964) A471.
[16] Olivier Delaire, Jie Ma, Karol Marty, Andrew F. May, Michael A. McGuire, Mao-Hua Du, David J. Singh, A. Podlesnyak, G. Ehlers, M.D. Lumsden, B.C. Sales, Giant anharmonic phonon scattering in PbTe, Nat. Mater. 10 (2011) 614–619.
[17] Xiaokun Gu, Yujie Wei, Xiaobo Yin, Baowen Li, Ronggui Yang, Colloquium: phononic thermal properties of two-dimensional materials, Rev. Mod. Phys. 90 (2018): 041002.
[18] Jie Chen, Xiangfan Xu, Jun Zhou, Baowen Li, Interfacial thermal resistance: past, present, and future, Rev. Mod. Phys. 94 (2022): 025002.
[19] Joon Sang Kang, Man Li, Huan Wu, Huuduy Nguyen, Yongjie Hu, Experimental observation of high thermal conductivity in boron arsenide, Science 361 (2018) 575–578.
[20] Sheng Li, Qiye Zheng, Yinchuan Lv, Xiaoyuan Liu, Xiqu Wang, Pinshane Y. Huang, David G. Cahill, Bing Lv, High thermal conductivity in cubic boron arsenide crystals, Science 361 (2018) 579–581.
[21] Fei Tian, Bai Song, Xi Chen, Navaneetha K. Ravichandran, Yinchuan Lv, Ke Chen, Sean Sullivan, Jaehyun Kim, Yuanyuan Zhou, Te-Huan Liu, Miguel Goni, Zhiwei Ding, Jingying Sun, Geethal Amila Gamage Udalamatta Gamage, Haoran Sun, Hamidreza Ziyaee, Shuyuan Huyan, Liangzi Deng, Jianshi Zhou, Aaron J. Schmidt, Shuo Chen, Ching-Wu Chu, Pinshane Y. Huang, David Broido, Li Shi, Gang Chen, Zhifeng Ren, Unusual high thermal conductivity in boron arsenide bulk crystals, Science 361 (2018) 582–585.
[22] Yinchang Zhao, Shuming Zeng, Geng Li, Chao Lian, Zhenhong Dai, Sheng Meng, Jun Ni, Lattice thermal conductivity including phonon frequency shifts and scattering rates induced by quartic anharmonicity in cubic oxide and fluoride perovskites, Phys. Rev. B 104 (2021): 224304.
[23] Tianli Feng, Xiulin Ruan, Higher-order phonon scattering: advancing the quantum theory of phonon linewidth, thermal conductivity and thermal radiative properties, in: *Nanoscale Energy Transport*, 2053-2563, IOP Publishing, 2020, 2–1, 2–44.
[24] Tianli Feng, Xiulin Ruan, Quantum mechanical prediction of four-phonon scattering rates and reduced thermal conductivity of solids, Phys. Rev. B 93 (2016): 045202.
[25] Xiaolong Yang, Tianli Feng, Li Ju, Xiulin Ruan, Stronger role of four-phonon scattering than three-phonon scattering in thermal conductivity of III-V semiconductors at room temperature, Phys. Rev. B 100 (2019): 245203.
[26] Qi Wang, Zezhu Zeng, Yue Chen, Revisiting phonon transport in perovskite $SrTiO_3$: anharmonic phonon renormalization and four-phonon scattering, Phys. Rev. B 104 (2021): 235205.
[27] L. Xie, J.H. Feng, R. Li, J.Q. He, First-principles study of anharmonic lattice dynamics in low thermal conductivity $AgCrSe_2$: evidence for a large resonant four-phonon scattering, Phys. Rev. Lett. 125 (2020): 245901.
[28] Xia Yi, Revisiting lattice thermal transport in PbTe: the crucial role of quartic anharmonicity, Appl. Phys. Lett. 113 (2018): 073901.
[29] Tianli Feng, Lucas Lindsay, Xiulin Ruan, Four-phonon scattering significantly reduces intrinsic thermal conductivity of solids, Phys. Rev. B 96 (2017): 161201.
[30] Ashis Kundu, Xiaolong Yang, Jinlong Ma, Tianli Feng, Jesús Carrete, Xiulin Ruan, Georg K.H. Madsen, Wu Li, Ultrahigh thermal conductivity of θ-phase tantalum nitride, Phys. Rev. Lett. 126 (2021): 115901.
[31] Charles Kittel, Introduction to Solid State Physics, Wiley, New York, 1976.
[32] Navaneetha K. Ravichandran, David Broido, Non-monotonic pressure dependence of the thermal conductivity of boron arsenide, Nat. Commun. 10 (2019) 827.
[33] L. Lindsay, D.A. Broido, Jesús Carrete, Natalio Mingo, T.L. Reinecke, Anomalous pressure dependence of thermal conductivities of large mass ratio compounds, Phys. Rev. B 91 (2015) 121202(R).
[34] Douglas Allen Dalton, Wen-Pin Hsieh, Gregory T. Hohensee, David G. Cahill, Alexander F. Goncharov, Effect of mass disorder on the lattice thermal conductivity of mgo periclase under pressure, Sci. Rep. 3 (2013) 2400.
[35] Guoqing Sun, Jinlong Ma, Chenhan Liu, Zheng Xiang, Dongwei Xu, Te-Huan Liu, Xiaobing Luo, Four-phonon and normal scattering in 2d hexagonal structures, Int. J. Heat Mass Tran. 215 (2023): 124475.
[36] L. Zaluski, A. Zaluska, J.O. Ström-Olsen, Hydrogenation properties of complex alkali metal hydrides fabricated by mechano-chemical synthesis, J. Alloys Compd. 290 (1999) 71–78.
[37] Gary Sandrock, James Reilly, Jason Graetz, Wei-Min Zhou, John Johnson, James Wegrzyn, Alkali metal hydride doping of α-AlH_3 for enhanced H_2 desorption kinetics, J. Alloys Compd. 421 (2006) 185–189.
[38] N.A.A. Rusman, M. Dahari, A review on the current progress of metal hydrides material for solid-state hydrogen storage applications, Int. J. Hydrog. Energy 41 (2016) 12108–12126.
[39] Hikaru Yamamoto, Hiroki Miyaoka, Satoshi Hino, Haruyuki Nakanishi, Takayuki Ichikawa, Yoshitsugu Kojima, Recyclable hydrogen storage system composed of ammonia and alkali metal hydride, Int. J. Hydrog. Energy 34 (2009) 9760–9764.
[40] Lyci George, Surendra K. Saxena, Structural stability of metal hydrides, alanates and borohydrides of alkali and alkali-earth elements: a review, Int. J. Hydrog. Energy 35 (2010) 5454–5470.
[41] M.A. Olea-Amezcua, O. De la Peña Seaman, R. Heid, Superconductivity by doping in alkali-metal hydrides without applied pressure: an *ab initio* study, Phys. Rev. B 99 (2019): 214504.
[42] G. Kresse, J. Furthmüller, Efficient iterative schemes for *ab initio* total-energy calculations using a plane-wave basis set, Phys. Rev. B 54 (1996) 11169–11186.

[43] John P. Perdew, Kieron Burke, Matthias Ernzerhof, Generalized gradient approximation made simple, Phys. Rev. Lett. 77 (1996) 3865–3868.
[44] Fei Zhou, Weston Nielson, Yi Xia, Vidvuds Ozoliņš, Lattice anharmonicity and thermal conductivity from compressive sensing of first-principles calculations, Phys. Rev. Lett. 113 (2014): 185501.
[45] Terumasa Tadano, Shinji Tsuneyuki, Self-consistent phonon calculations of lattice dynamical properties in cubic $SrTiO_3$ with first-principles anharmonic force constants, Phys. Rev. B 92 (2015): 054301.
[46] Zherui Han, Xiaolong Yang, Wu Li, Tianli Feng, Xiulin Ruan, Fourphonon: an extension module to shengbte for computing four-phonon scattering rates and thermal conductivity, Comput. Phys. Commun. 270 (2022): 108179.
[47] Tianli Feng, Xiaolong Yang, Xiulin Ruan, Phonon anharmonic frequency shift induced by four-phonon scattering calculated from first principles, J. Appl. Phys. 124 (2018): 145101.
[48] Xia Yi, Vinay I. Hegde, Koushik Pal, Xia Hua, Dale Gaines, Shane Patel, Jiangang He, Muratahan Aykol, Chris Wolverton, High-throughput study of lattice thermal conductivity in binary rocksalt and zinc blende compounds including higher-order anharmonicity, Phys. Rev. X 10 (2020): 041029.
[49] R. Thomas, Koehler, "Theory of the self-consistent harmonic approximation with application to solid neon,", Phys. Rev. Lett. 17 (1966) 89–91.
[50] Xiaoying Wang, Zhibin Gao, Guimei Zhu, Jie Ren, Lei Hu, Jun Sun, Xiangdong Ding, Yi Xia, Baowen Li, Role of high-order anharmonicity and off-diagonal terms in thermal conductivity: a case study of multiphase $CsPbBr_3$, Phys. Rev. B 107 (2023): 214308.
[51] A.W. Szafranski, E. Keller, E.U. Franck, Thermodynamics of liquid cesium-cesium hydride mixtures at high pressures and temperatures, Phys. Chem. 96 (1992) 955–962.
[52] N.R. Werthamer, Self-consistent phonon formulation of anharmonic lattice dynamics, Phys. Rev. B 1 (1970) 572.
[53] Atsushi Togo and Isao Tanaka, "First principles phonon calculations in materials science,", Scripta Mater. 108 (2015) 1–5.
[54] L. Lindsay, Isotope scattering and phonon thermal conductivity in light atom compounds: LiH and LiF, Phys. Rev. B 94 (2016): 174304.
[55] Xiaokun Gu, C.Y. Zhao, Thermal conductivity of hexagonal Si, Ge, and $Si_{1-x}Ge_x$ alloys from first-principles, J. Appl. Phys. 123 (2018): 185104.
[56] Mattia Sist, Karl Frederik Færch Fischer, Hidetaka Kasai, Bo Brummerstedt Iversen, Low-temperature anharmonicity in cesium chloride (CsCl), Angew. Chem. 129 (2017) 3679–3683.
[57] Wei Bin, Xiaoxia Yu, Chao Yang, Xin Rao, Xueyun Wang, Songxue Chi, Xuefeng Sun, Jiawang Hong, Low-temperature anharmonicity and the thermal conductivity of cesium iodide, Phys. Rev. B 99 (2019): 184301.
[58] Wei Bin, Xiaoxia Yu, Chao Yang, Xin Rao, Xueyun Wang, Songxue Chi, Xuefeng Sun, Jiawang Hong, Low-temperature anharmonicity and the thermal conductivity of cesium iodide, Phys. Rev. B 99 (2019): 184301.
[59] Zhen Tong, Xiaolong Yang, Tianli Feng, Hua Bao, Xiulin Ruan, First-principles predictions of temperature-dependent infrared dielectric function of polar materials by including four-phonon scattering and phonon frequency shift, Phys. Rev. B 101 (2020): 125416.
[60] Michele Lazzeri, Matteo Calandra, Francesco Mauri, Anharmonic phonon frequency shift in mgb 2, Phys. Rev. B 68 (2003): 220509.
[61] Deane K. Smith, H.R. Leider, Low-temperature thermal expansion of lih, mgo and cao, J. Appl. Crystallogr. 1 (1968) 246–249.